AIP Journal of Applied Physics

Reliability assessment and degradation analysis of 1.3 m GaInNAs lasers

W. Lu, S. Bull, J. J. Lim, R. MacKenzie, S. Sujecki, A. V. Andrianov, M. Sadeghi, S. M. Wang, A. Larsson, P. Melanen, P. Sipilä, P. Uusimaa, C. T. Foxon, and E. C. Larkins

Citation: Journal of Applied Physics **106**, 093110 (2009); doi: 10.1063/1.3256156
View online: http://dx.doi.org/10.1063/1.3256156
View Table of Contents: http://scitation.aip.org/content/aip/journal/jap/106/9?ver=pdfcov
Published by the AIP Publishing

Reliability assessment and degradation analysis of 1.3 μm GaInNAs lasers

W. Lu,[1,a)] S. Bull,[1] J. J. Lim,[1] R. MacKenzie,[1] S. Sujecki,[1] A. V. Andrianov,[1] M. Sadeghi,[2] S. M. Wang,[2] A. Larsson,[2] P. Melanen,[3] P. Sipilä,[3] P. Uusimaa,[3] C. T. Foxon,[4] and E. C. Larkins[1]

[1]*Photonic and Radio Frequency Engineering Group (PRFEG), Electrical Systems and Optics Research Division, Faculty of Engineering, University of Nottingham, Nottingham NG7 2RD, United Kingdom*
[2]*Department of Microtechnology and Nanoscience, Photonics Laboratory, Chalmers University of Technology, S-412 96 Göteborg, Sweden*
[3]*Modulight Inc., P.O. Box 770, 33101 Tampere, Finland*
[4]*School of Physics and Astronomy, University of Nottingham, Nottingham NG7 2RD, United Kingdom*

(Received 19 September 2009; accepted 30 September 2009; published online 12 November 2009)

The degradation of 1.3 μm GaInNAs lasers was investigated using accelerated aging tests. This was followed by comprehensive characterization, including standard light-current-voltage (L-I-V) characterization, capacitance measurements, photoluminescence microscopy (PLM), on-axis amplified spontaneous emission (ASE) spectra measurements, and photocurrent (PC) and electroluminescence (EL) spectroscopies. The slope efficiency of the device dropped by 50% with a 300% increase in the threshold current after the accelerated aging test. The ideality factors of the aged devices are higher than those of the unaged devices. PLM images showed no evidence of catastrophic optical mirror damage. The measured capacitances of the aged devices are all similar to those of the unaged devices, indicating that there was no significant dopant diffusion in the junction region. Fourier transforms of the ASE spectra showed that no intracavity defects were present in the aged lasers, suggesting that intracavity defects are not responsible for the rapid degradation of the aged devices. Although the PC measurements showed defects at 0.88–0.95 eV and at ~0.76 eV, these defect signatures did not increase with aging. On the other hand, EL measurements revealed that radiative deep level defects were generated during the aging tests, which may be related to the degradation of the devices. Based on the above measurement results, we identify the generation of radiative deep level defects as the main causes of degradation of these devices. © *2009 American Institute of Physics*. [doi:10.1063/1.3256156]

I. INTRODUCTION

Kondow *et al.*[1] proposed GaInNAs for 1.3 μm GaAs-based lasers in 1996. Since then, great effort has been made to improve the performance of GaInNAs quantum well (QW) lasers, grown by both molecular beam epitaxy (MBE)[2–5] and metal-organic vapor phase epitaxy.[6–9] Recently, state-of-the-art GaInNAs edge-emitting lasers (EELs) have demonstrated a great deal of promise as a low-cost replacement for directly modulated 1.3 μm InP devices for access network applications. Lasers based on the GaInNAs/GaAs material system have a large conduction band offset, which increases the electron confinement and subsequently reduces their temperature sensitivity. Some of the best performance characteristics demonstrated so far are a low threshold current density of 300 A/cm^2,[10] a high characteristic temperature of up to 200 K,[11] a 3 dB modulation bandwidth of 17 GHz at 25 °C,[12] and the ability to be directly modulated up to 10 Gbytes/s at a heat sink temperature of 110 °C.[13]

Despite the rapid development in the growth of dilute nitride lasers, there are only a few reports on the reliability of MBE-grown GaInNAs lasers.[14,15] Kondow *et al.*[4] provided the first report about the potential reliability of GaAs-based GaInNAs 1.3 μm lasers grown by gas-source MBE in 1999. The 3.6×800 μm^2 single QW laser was mounted epitaxial side upwards and survived 1000 h at 24 °C under an autocurrent-control condition (~4.5 kA/cm^2). Both facets of the device were coated with high reflectivity (HR) coatings (70% and 95%, respectively) using SiO_2 and amorphous Si. After the aging test, the slope efficiency decreased by 9% from 0.066 to 0.060 W/A and the lasing wavelength blue-shifted less than 1 nm. Livshits *et al.*[2] reported an aging test of a 1.3 μm $Ga_{0.64}In_{0.36}N_{0.0154}As_{0.9846}/GaN_{0.0224}As_{0.9776}$ QW laser grown by solid-source MBE, which had been operated for >2500 h at a temperature of 124 °C at a pulsed (1% duty cycle) output power of 1.5 W. The authors suggested that this corresponded to a current density of 30 kA/cm^2 and upwards of 1000 h of operation at 1.5 W of a continuous wave (cw) output power at 35 °C. Antireflective (5%) and HR (99%) coatings were used on the facets. No noticeable degradation was observed after thermal stressing. This test showed that GaInNAs-based devices had the potential as an active material for reliable high power lasers, and could reliably meet the operating temperature ranges required for commercial deployment. Prakash *et al.*[15] also demonstrated excellent reliability of 1.25–1.3 μm GaInNAs vertical cavity surface emitting lasers grown by MBE. After operating at a current density of 28 kA/cm^2 at 110 °C (0.8–1 mW) for 8000 h, no failures were observed. However, the devices began to fail after ~2500 h, when they were

[a)]Electronic mail: eexwl3@nottingham.ac.uk. FAX: +44 (0)115 951 5616.

operated at 30 kA/cm^2 at 124 °C (0.8–1 mW). The authors also investigated the wearout mechanisms using electroluminescence (EL) and cross-sectional transmission electron microscopy. Dark line defects (DLDs) and dark spot defects (DSDs) were both observed in the devices that failed. DLDs along the ⟨100⟩ directions were observed in (and confined to) the active region. The authors postulated that DSDs correspond to point defects from which DLDs grow during operation. Additionally, the failed devices exhibited multimode behavior during failure. The output wavelength of the failed devices blueshifted more (1.2 nm) than those devices that survived the life testing (~0.8 nm).[15]

Although reliability does not present any fundamental limits to the viability of GaInNAs lasers, the dominant degradation mechanism for these devices remains unclear. In this paper, we report on accelerated aging tests and a range of measurements to investigate the degradation of 1.3 μm GaInNAs EELs. These measurements include standard light-current-voltage (L-I-V) characterization, capacitance measurements, photoluminescence microscopy (PLM), on-axis amplified spontaneous emission (ASE) spectrum measurements, and photocurrent (PC) and EL measurements. The paper is organized as follows: Section II describes the aging process and experimental techniques used in our investigations and provides details of the laser structures studied. In Sec. III, the characterization results are presented and analyzed. Finally, in Sec. IV, we draw our conclusions.

II. EXPERIMENT

The lasers used in this study are GaInNAs-based double QW devices, which were grown using an EPI930 SS MBE system with a load-locked rf nitrogen plasma source. The layer structure is shown in Fig. 1. After capping the first QW with 10 nm GaAs, the growth was stopped and the sample was annealed at 600 °C for 10 min (the location of the growth interruption is labeled with a thick line in Fig. 1). No postgrowth annealing was applied. Be and Si were used as *p*- and *n*-dopants, respectively. A 2 μm wide, 300 μm long ridge was fabricated by reactive ion etching using silicon tetrachloride ($SiCl_4$) as the process gas. Ti–Pt–Au was used for the *p*-contact and Au–Ge–Au for the *n*-contact. 70% and 30% optical coatings were applied to the back and front facets, respectively. The In and N contents were calculated using dynamical diffraction analysis of high-resolution x-ray diffraction.

The accelerated aging tests were performed under autopower-control conditions. The test conditions were selected to be 6 mW constant operating power at 70 °C with a failure criterion of a 50% increase in the threshold current.

The cw L-I and I-V characteristics of the devices were measured. The capacitance of each device was measured at zero bias. PLM measurements were performed in the system detailed in Ref. 16. On-axis ASE spectra were collected by a single-mode fiber for measurement with an optical spectrum analyzer, as described in Ref. 17. PC spectroscopy measurements were carried out using a 250 W halogen lamp as the excitation source. Monochromatic light was generated by a 1 m Hilger–Watt monochromator with a spectral resolution of

Layer Type	Layer Thickness (nm)	Material	Growth Temperature (°C)	Doping (cm^{-3})
p^{++} Contact	100	GaAs	580	2×10^{19}
p-Grading	200	$Al_{0.2}Ga_{0.8}As$-- $Al_{0.5}Ga_{0.5}As$	700	2×10^{19}-- 5×10^{17}
p-Cladding	1000	$Al_{0.5}Ga_{0.5}As$	700	5×10^{17}
GRIN WG	160	$Al_{0.5}Ga_{0.5}As$-- $Al_{0.2}Ga_{0.8}As$	700	Intrinsic
SCH Layer	40	GaAs	580	Intrinsic
QW	7	$Ga_{0.613}In_{0.387}As_{0.988}N_{0.012}$	450	Intrinsic
Barrier	10	GaAs	580	Intrinsic
Barrier	10	GaAs	580	Intrinsic
QW	7	$Ga_{0.613}In_{0.387}As_{0.988}N_{0.012}$	450	Intrinsic
SCH Layer	40	GaAs	580	Intrinsic
GRIN WG	160	$Al_{0.5}Ga_{0.5}As$-- $Al_{0.2}Ga_{0.8}As$	700	Intrinsic
n-Cladding	1000	$Al_{0.5}Ga_{0.5}As$	700	5×10^{17}
n-Grading	200	$Al_{0.2}Ga_{0.8}As$-- $Al_{0.5}Ga_{0.5}As$	700	5×10^{17}-- 4×10^{18}
Superlattice	10/10×10	GaAs/AlAs	580	4×10^{18}
n^{++} Buffer	300	GaAs	580	4×10^{18}
n^{+} (100) GaAs Substrate				

FIG. 1. Laser layer structure showing the materials, thicknesses, growth temperatures, and doping levels.

3 nm. By using a microscope objective, the excitation spot size could be as small as ~5 μm. A Keithley 428 current amplifier was used to preamplify the resultant PC signal, which was measured using a Stanford Research System SR830 lock-in amplifier. EL spectroscopy measurements were performed under cw conditions with a 50 mA driven current. The dispersed EL signal was collected by a liquid nitrogen cooled Ge detector. All measurements were performed at 300 K.

III. RESULTS AND DISCUSSION

Three devices (008-10, 019-08, and 017-05) were not subjected to the aging test and four devices (020-08, 017-14,

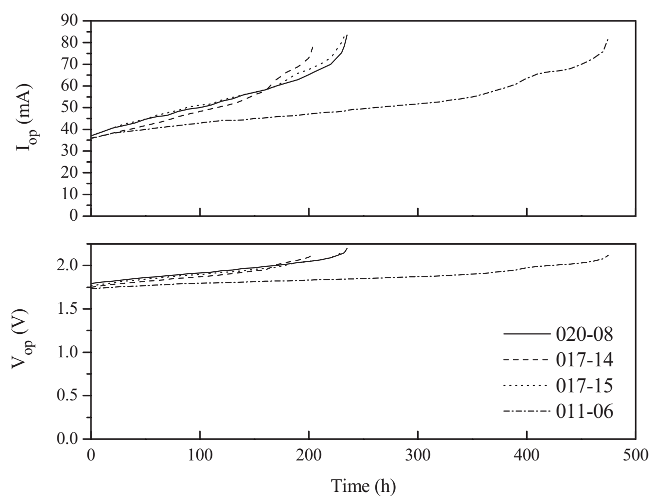

FIG. 2. Evolution of the operating current and the operating voltage during the 6 mW constant power aging test at 70 °C.

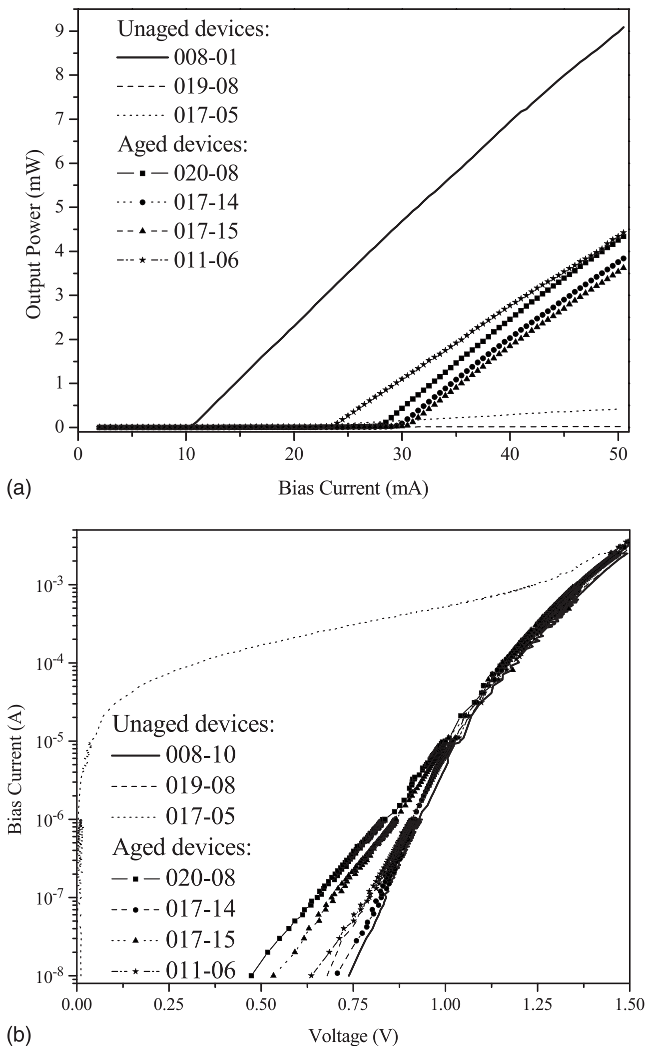

FIG. 3. (a) L-I and (b) I-V characteristics of the mounted (unaged and aged) devices at 300 K.

017-15, and 011-06) were aged later. Following mounting, four devices were subjected to a constant power accelerated aging test at 6 mW and an elevated temperature of 70 °C. After 200–500 h, all devices reached the failure criterion. Figure 2 shows the evolution of the operating current and operating voltage during the aging test, respectively. The operating voltage follows the change in the operating current. Device 011-06 had the lowest threshold current density and the longest survival time of the aged devices.

Figure 3(a) and 3(b) show the cw L-I and I-V characteristics of the mounted devices (aged and unaged). The threshold current density and the slope efficiency were extracted for each device from these characteristics. The threshold current density and slope efficiency of each device were also measured prior to mounting. Table I shows the values of these parameters. All of the devices had similar behavior before mounting and aging, but the L-I characteristics of the devices after mounting and aging differed significantly. As seen in Table I, the unaged devices had a higher threshold current density and lower slope efficiency after mounting than they did before mounting. This suggests that the mounting process damaged the devices. All of the aged devices have a significantly higher threshold current density (approximately three times larger) and lower slope efficiency. Experimental study[18] and theoretical models[19] show that nonradiative recombination dominates the threshold current at room temperatures. This suggests that such a large increase in the threshold current density indicates an increase in the nonradiative recombination rate. The ideality factors of the aged devices at low current densities are slightly higher than those of the unaged devices, which is consistent with an increase in the nonradiative recombination rate after aging. (Note that device 019-08 and device 017-05 are damaged, so their ideality factors are not reliable.)

The capacitance of each device was measured under zero bias and the results are given in Table I. The measured capacitances of the aged devices are all similar to those of the unaged devices. This indicates that there was no significant dopant diffusion in the junction region.

PLM is a sensitive technique to detect catastrophic optical mirror damage (COMD) of the laser facets. Although PLM images were taken from the front facets of all unaged and aged devices, no evidence of COMD was found. This indicates that COMD was not responsible for their failure.

Intracavity defects are physically line defects or defect complexes and have been associated with rapid degradation.[20] Such defects and their positions within a Fabry–Pérot laser diode can be revealed by examining the ASE spectrum below threshold.[21,22] This technique requires a high-resolution measurement of the ASE spectrum, which clearly resolves the individual Fabry–Pérot resonances. A Fourier transform is performed on the ASE spectrum, which is then scaled with the expression

TABLE I. Summary of the threshold currents and slope efficiencies of the unmounted and mounted devices, and the ideality factors and capacitances of the mounted devices at 300 K.

	Unmounted		Mounted				
Serial No.	J_{th} (kA/cm^2)	Slope efficiency (W/A)	J_{th} (kA/cm^2)	Slope efficiency (W/A)	Ideality factor	Capacitance (pF)	Aged
008-10	1.54	0.366	1.75	0.227	2.61	14.0	No
019-08	1.76	0.340	>8.33	⋯	3.17	15.5	No
017-05	1.46	0.384	3.25	0.014	≈0	17.5	No
020-08	1.68	0.375	4.63	0.191	4.94	15.4	Yes
017-14	1.68	0.378	4.92	0.179	3.52	16.0	Yes
017-15	1.72	0.376	5.05	0.177	4.51	16.0	Yes
011-06	1.48	0.373	3.92	0.162	3.49	14.0	Yes

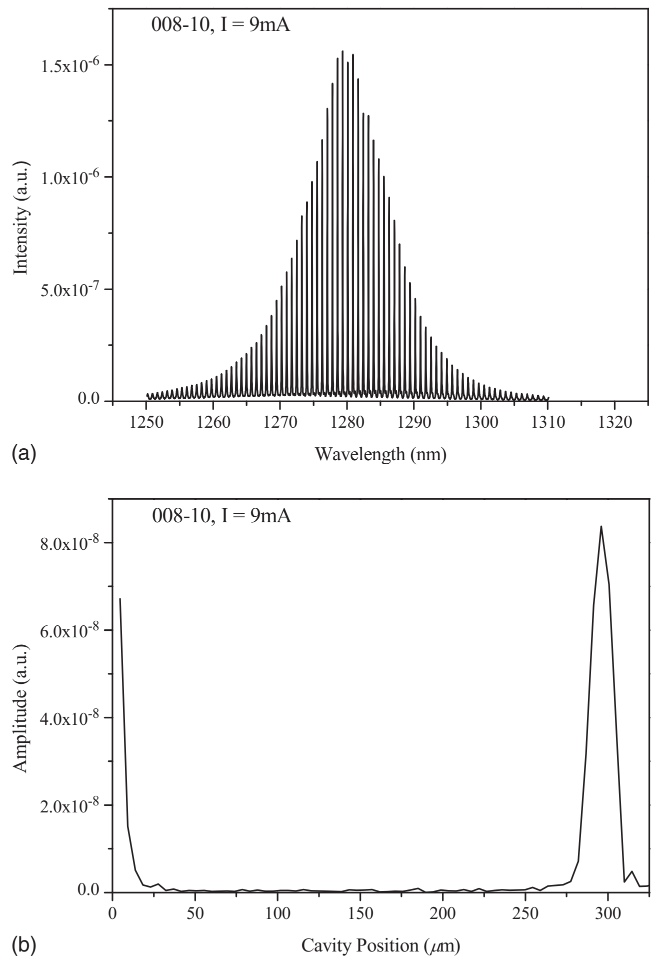

FIG. 4. Measured (a) ASE spectrum and (b) the corresponding Fourier transform from device 008-10.

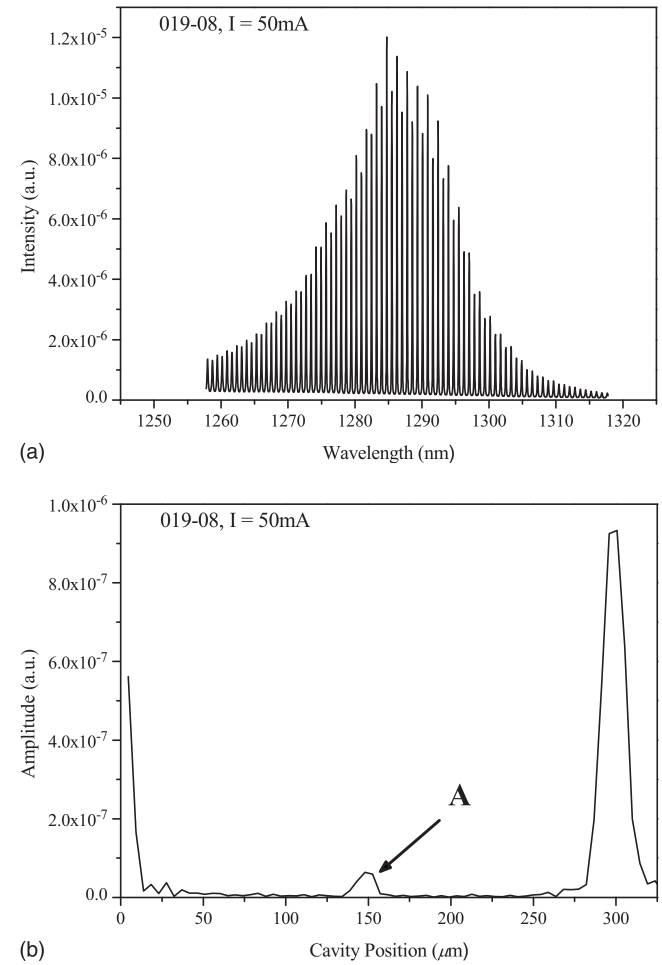

FIG. 5. Measured (a) ASE spectrum and (b) the corresponding Fourier transform from device 019-08.

$$L = \frac{\lambda^2}{2n_g\Delta\lambda}, \tag{1}$$

where L is the cavity length, λ is the peak wavelength, $\Delta\lambda$ is the mode spacing, and n_g is the effective group index. The resulting Fourier transform has a large peak corresponding to the dc frequency component of the spectrum and another peak corresponding to the length of the cavity. For a defect-free cavity, only one resonance should occur at the position equal to the cavity length. Resonances that occur at other cavity positions indicate perturbations/defects within the cavity.

The ASE spectra from all of the devices (unaged and aged) were measured at a current just under the threshold current. The ASE spectra were examined for defects/features via both visual inspection and using the Fourier analysis method described above. The majority of the ASE spectra appear as expected and are similar to that from device 008-10, shown in Fig. 4(a). Figure 4(b) shows the corresponding Fourier transform of the spectrum. An intracavity defect was only observed in one device, which was visibly damaged (as discussed below). Thus, intracavity defects do not appear to be responsible for the rapid degradation of these devices. This is consistent with our earlier PLM studies of highly strained GaInNAs samples, which did not show the formation of misfit dislocations even after annealing.[23] Both results can be understood in terms of the pinning of dislocations by the localized strain field of the nitrogen impurities.

An intracavity peak was only observed in device 019-08. The peak is located at the center of the cavity at 150 μm (feature A), as shown in Fig. 5(b). This is an unaged device, but as referred to in Table I, the device was still below the threshold current density at 8.33 kA/cm^2 (whereas the threshold density before dicing and mounting was 1.76 kA/cm^2). Thus, there is clearly significant current leakage, possibly through the defect identified at 150 μm. Figure 6 shows a photograph of this device, where a damaged region can be observed near the wire bond at the midpoint of the cavity. As this defect did not result from aging-induced degradation, it may be due to damage during the packaging.

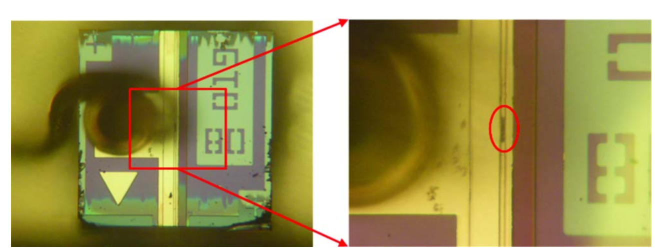

FIG. 6. (Color online) Top views of device 019-08. A damaged region is clearly seen in the center of the cavity.

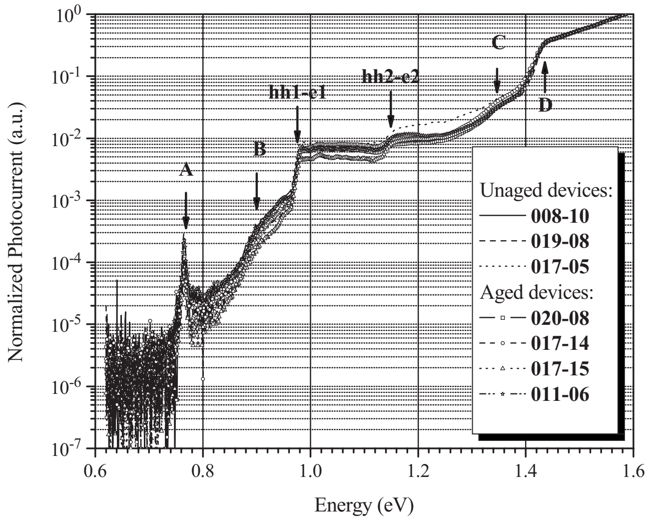

FIG. 7. Normalized PC spectra for the unaged and aged devices at 300 K. (The arrows show the calculated QW transition energies.)

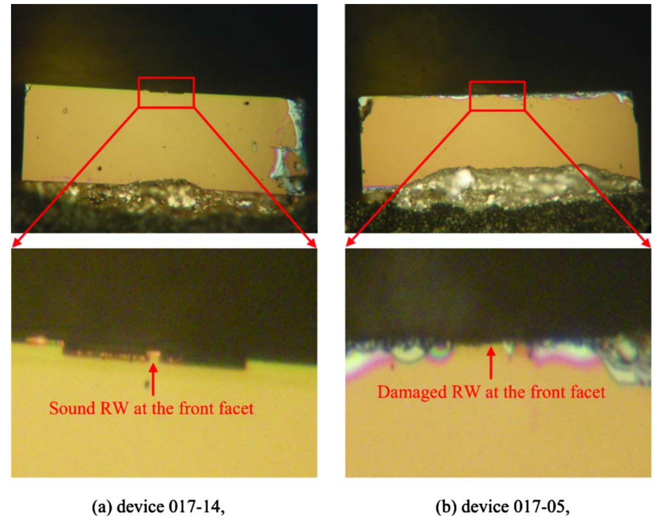

FIG. 8. (Color online) Front views of (a) device 017-14 and (b) device 017-05. A damaged RW at the front facet of device 017-05 is clearly seen.

PC spectroscopy has been used to analyze the aging of laser diodes and provide insight into their microscopic degradation mechanisms.[24,25] In general, the PC signal is determined by the absorption spectrum of the device, the mechanism affecting the separation of electrons and holes, and the diffusion and recombination of the photogenerated carriers.

Figure 7 presents the PC spectra of unaged and aged devices plotted on a semilogarithmic scale. The absolute values of photometric data are difficult to determine, so we use the PC value at 1.59 eV as a reference point for normalization. (This photon energy was selected because the spectral envelope does not differ significantly in the 1.4–1.6 eV range. This PC signal mainly originates from GaAs layers, which are less affected by aging effects than the QW.) The spectra in Fig. 7 extend over a signal range of five orders of magnitude with an excellent signal-to-noise ratio. There are three notable features in the PC spectra: (i) a weak sharp peak centered around 0.76 eV (labeled A), (ii) a broad shoulder extending from about 0.88 to 0.95 eV (labeled B), and (iii) strong components between 0.95 and 1.6 eV. The first two features indicate that at least two different types of defect exist in the devices: (i) a deep level located at 0.76 eV below the QW conduction band or above the QW valence band, which could be a hole trap[26] or an electron trap;[27,28] (ii) shallower states in the band gap (0.88–0.95 eV), which may be attributed to oxygen-related defects in GaAs barriers.[29] The third feature contains four steplike signals, which correspond to the first heavy hole to the first conduction band transition (hh1-e1) in the QW, the second heavy hole to the second conduction band transition (hh2-e2) in the QW, the shallow states in the bandgap of GaAs (labeled C), and the valence band to the conduction band transition of the GaAs layer (labeled D), respectively. Upon aging, the third signal component does not change significantly, which indicates that the band gap energies of the GaAs confinement layer and GaInNAs QWs are the same for the aged and unaged devices. Furthermore, this suggests that there is no aging-induced change in the strain, composition, or N-bonding configuration in the QWs. The magnitudes of the “A” and “B” defects do not appear to have changed much during the aging process, suggesting that they are not responsible for the rapid degradation of the devices. There is data dispersion between 1.15 and 1.4 eV from device 017-05 and between 1.0 and 1.15 eV from device 017-15. Figure 8 shows the photographs of the ridge waveguides (RWs) at the front facets of devices 017-14 and 017-05. The damaged RW at the front facet may influence the absorption efficiency of the devices and cause such dispersion.

The defects revealed by the PC measurements are not necessarily responsible for the degradation of the devices. PC spectroscopy relies on absorption, and the intensity of incident photons may be too low to reveal defects with a low density. On the other hand, EL spectroscopy can reveal radiative transitions from defects—even if the defect volume density is too small to be seen by the PC spectroscopy.

Figure 9 shows the front facet EL spectra of all samples plotted on a semilogarithmic scale and normalized to their minimum values. The devices were biased with a dc of 50 mA. The EL spectra of devices 019-08 and 017-05 do not show lasing characteristics. This is because of damage to the RW at the midpoint of the cavity in device 019-08 and at the front facet of device 017-05. Devices 008-10, 020-08, 017-14, 017-15, and 011-06 clearly show lasing spectra. In the following analysis, we focus on the EL spectra in the low and high energy tails, as shown in Fig. 10. Broad peaks are observed in the high energy tails of the EL spectra between 1.10 and 1.35 eV. Since their energies are larger than the fundamental transition energy of the QW, these transitions should come from the barriers or cladding layers. The defects related to these transitions probably are not responsible for the device degradation, because their positions and magnitudes are almost the same for the unaged and aged devices. (Note that these peaks are not observed in the EL spectra of devices 019-08 and 017-05, possibly for the same reason that these devices do not lase.) However, there are obvious differences between the unaged and aged devices in the low energy tails of the EL spectra. With aging, broad peaks appear in the low energy tails of the EL spectra between 0.79

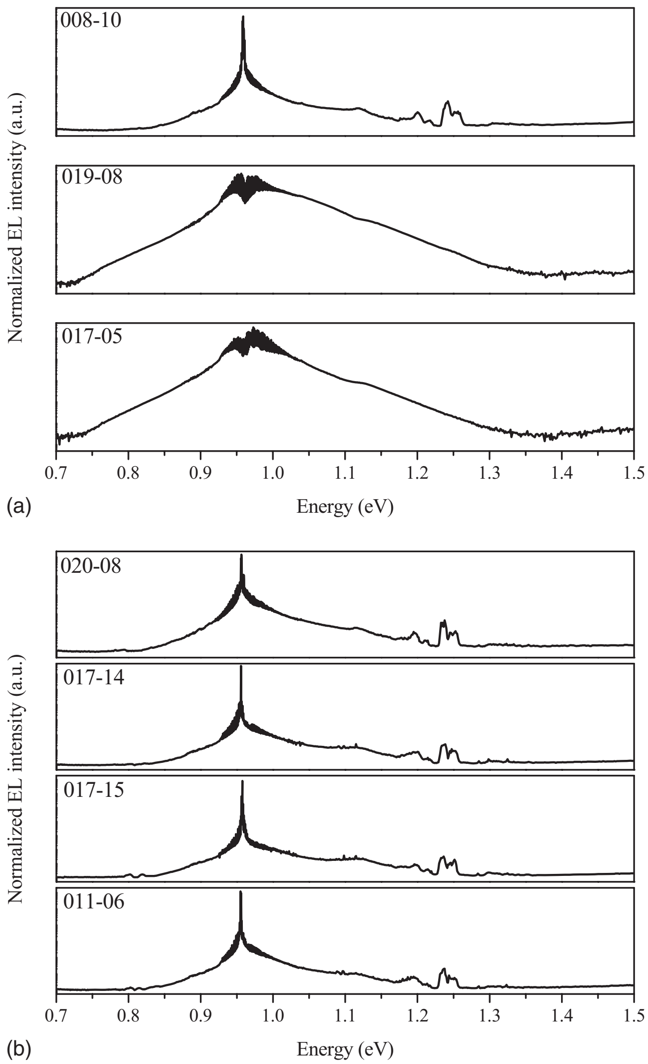

FIG. 9. Normalized EL spectra of (a) unaged devices and (b) aged devices at 300 K.

and 0.84 eV. The radiative defects related to these peaks are located close to the QW band edges, which may be the native arsenic antisite (As_{Ga}) such as EL2 in GaAs.[30] These defects also may be the N-dimer split interstitial defects, i.e., two N atoms on a single As site [$(N-N)_{As}$], which are located around 0.8 eV above the QW valence band edge.[31,32] This thermal activation energy is within the range of the peak positions in the low energy tails of the EL spectra. The defects related to these peaks seem to be responsible for the device degradation. They are not observed in the PC spectra probably due to their low defect densities. Further investigations are needed to identify the microscopic nature of these defects in the low energy tail of the EL spectrum.

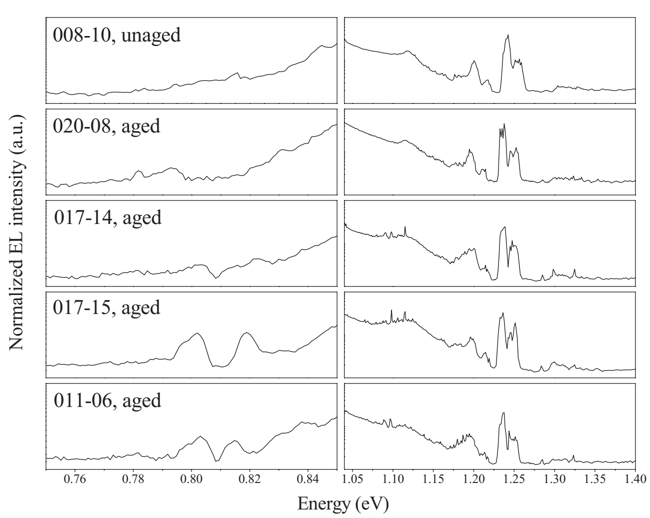

FIG. 10. Normalized EL spectra in the low and high energy tails.

IV. CONCLUSIONS

A range of measurements were performed to investigate the degradation of 1.3 μm GaInNAs lasers. The ideality factors of the aged devices are higher than those of the unaged devices, suggesting that the nonradiative recombination increases after aging. There was no significant dopant diffusion in the junction region, as seen from the capacitances of the aged devices, which are all similar to those of the unaged devices. PLM shows no evidence of COMD. Intracavity defects do not seem to be responsible for the rapid device degradation, since Fourier transforms of the ASE spectra show no intracavity peak in the aged devices. Damage to the RW at the front facet was observed, which may contribute to the increased threshold current. The defect signatures from the PC measurements do not increase with aging. On the other hand, EL measurements show that radiative deep level defects are generated during aging, which may be related to the degradation of the devices. Based on these measurement results, we conclude that the generation of radiative deep level defects plays a key role in the degradation of these devices.

[1]M. Kondow, K. Uomi, A. Niwa, T. Kitatani, S. Watahiki, and Y. Yazawa, Jpn. J. Appl. Phys., Part 1 **35**, 1273 (1996).
[2]D. A. Livshits, A. Egorov, and H. Riechert, Electron. Lett. **36**, 1381 (2000).
[3]W. Li, T. Jouhti, C. S. Peng, J. Konttinen, P. Laukkanen, E. M. Pavelescu, M. Dumitrescu, and M. Pessa, Appl. Phys. Lett. **79**, 3386 (2001).
[4]C. S. Peng, T. Jouhti, P. Laukkanen, E. M. Pavelescu, J. Konttinen, W. Li, and M. Pessa, IEEE Photonics Technol. Lett. **14**, 275 (2002).
[5]W. Ha, V. Gambin, M. Wistey, S. Bank, S. Kim, and J. S. Harris, Jr., IEEE Photonics Technol. Lett. **14**, 591 (2002).
[6]F. Hohnsdorf, J. Koch, S. Leu, W. Stolz, B. Borchert, and M. Druminski, Electron. Lett. **35**, 571 (1999).
[7]S. Sato, Jpn. J. Appl. Phys., Part 1 **39**, 3403 (2000).
[8]M. Kawaguchi, T. Miyamoto, E. Gouardes, D. Schlenker, T. Kondo, F. Koyama, and K. Iga, Jpn. J. Appl. Phys., Part 2 **40**, L744 (2001).
[9]N. Tansu, N. J. Kirsch, and L. Mawst, Appl. Phys. Lett. **81**, 2523 (2002).
[10]Y. Q. Wei, M. Sadeghi, S. M. Wang, P. Modh, and A. Larsson, Electron. Lett. **41**, 1328 (2005).
[11]Y. Q. Wei, J. S. Gustavsson, M. Sadeghi, S. M. Wang, A. Larsson, P. Savolainen, P. Melanen, and P. Sipila, Opt. Express **14**, 2753 (2006).
[12]Y. Q. Wei, J. S. Gustavsson, M. Sadeghi, S. M. Wang, and A. Larsson, IEEE J. Quantum Electron. **42**, 1274 (2006).
[13]J. S. Gustavsson, Y. Q. Wei, M. Sadeghi, S. M. Wang, and A. Larsson, Electron. Lett. **42**, 925 (2006).
[14]M. Kondow, T. Kitatani, K. Nakahara, and T. Tanaka, Jpn. J. Appl. Phys., Part 2 **38**, L1355 (1999).
[15]S. Prakash, L. Chirovsky, R. Naone, D. Galt, D. Kisker, and A. Jackson, Proc. SPIE **4994**, 44 (2003).
[16]S. Bull, A. V. Andrianov, I. Harrison, M. Dorin, R. B. Kerr, J. Noto, and E. C. Larkins, IEEE Trans. Instrum. Meas. **54**, 1079 (2005).
[17]R. MacKenzie, J. J. Lim, S. Bull, S. Chao, S. Sujecki, M. Sadeghi, S. M. Wang, A. Larsson, P. Melanen, P. Sipilä, P. Uusimaa, and E. C. Larkins, IET Proc. Optoelectron. **1**, 284 (2007).
[18]R. Fehse, S. Tomic, A. R. Adams, S. J. Sweeney, E. P. O'Reilly, A. Andreev, and H. Riechert, IEEE J. Sel. Top. Quantum Electron. **8**, 801

(2002).
[19]J. J. Lim, R. MacKenzie, S. Sujecki, M. Sadeghi, S.M. Wang, Y. Q. Wei, J. S. Gustavsson, A. Larsson, P. Melanen, P. Sipilä, P. Uusimaa, A. A. George, and E. C. Larkins, IET Proc. Optoelectron. **1**, 259 (2007).
[20]*Quantum-Well Laser Array Packaging*, edited by J. W. Tomm and J. Jiménez (McGraw-Hill, London, 2006).
[21]A. Klehr, G. Beister, G. Erbert, A. Klein, J. Maege, I. Rechenberg, J. Sebastian, H. Wenzel, and G. Tränkle, J. Appl. Phys. **90**, 43 (2001).
[22]P. J. Bream, S. Bull, I. Harrison, S. Sujecki, and E. C. Larkins, Appl. Phys. Lett. **86**, 061104 (2005).
[23]W. Lu, S. Chao, S. Bull, A. V. Andrianov, V. A. Grant, R. P. Campion, C. T. Foxon, M. Sadeghi, S. M. Wang, A. Larsson, and E. C. Larkins, Phys. Status Solidi C **5**, 467 (2008).
[24]A. V. Andrianov, S. R. A. Dods, J. Morgan, J. W. Orton, T. M. Benson, I. Harrison, E. C. Larkins, F. X. Daiminger, E. Vassilakis, and J. P. Hirtz, J. Appl. Phys. **87**, 3227 (2000).
[25]J. W. Tomm, A. Bärwolf, U. Menzel, M. Voss, R. Puchert, Th. Elsaesser, F. X. Daiminger, S. Heinemannn, and J. Luft, J. Appl. Phys. **81**, 2059 (1997).
[26]D. Kwon, R. J. Kaplar, S. A. Allerman, S. R. Kurtz, and E. D. Jones, Appl. Phys. Lett. **74**, 2830 (1999).
[27]R. J. Kaplar, A. R. Arehart, S. A. Ringel, A. A. Allerman, R. M. Sieg, and S. R. Kurtz, J. Appl. Phys. **90**, 3405 (2001).
[28]J. F. Chen, R. S. Hsiao, P. C. Hsieh, Y. C. Chen, J. S. Wang, and J. Y. Chi, J. Appl. Phys. **45**, 5662 (2006).
[29]H. Ch. Alt, Appl. Phys. Lett. **54**, 1445 (1989).
[30]D. V. Lang, A. Y. Cho, A. C. Gossard, M. Ilegenms, and W. Wiegmann, J. Appl. Phys. **47**, 2558 (1976).
[31]P. Krispin, V. Gambin, J. S. Harris, and K. H. Ploog, J. Appl. Phys. **93**, 6095 (2003).
[32]L. L. Goddard, S. R. Bank, M. A. Wistey, H. B. Yuen, Z. Rao, and J. S. Harris, Jr., J. Appl. Phys. **97**, 083101 (2005).